JACS
JOURNAL OF THE AMERICAN CHEMICAL SOCIETY
pubs.acs.org/JACS
Article

Force-Dependent Interactions between Talin and Full-Length Vinculin

Yinan Wang, Mingxi Yao, Karen B. Baker, Rosemarie E. Gough, Shimin Le, Benjamin T. Goult,* and Jie Yan*

Cite This: J. Am. Chem. Soc. 2021, 143, 14726−14737
Read Online
ACCESS | Metrics & More | Article Recommendations | Supporting Information

ABSTRACT: Talin and vinculin are part of a multicomponent system involved in mechanosensing in cell-matrix adhesions. Both exist in autoinhibited forms, and activation of vinculin requires binding to mechanically activated talin, yet how forces affect talin's interaction with vinculin has not been investigated. Here by quantifying the kinetics of force-dependent talin−vinculin interactions using single-molecule analysis, we show that mechanical exposure of a single vinculin binding site (VBS) in talin is sufficient to relieve the autoinhibition of vinculin, resulting in high-affinity binding. We provide evidence that the vinculin undergoes dynamic fluctuations between an autoinhibited closed conformation and an open conformation that is stabilized upon binding to the VBS. Furthermore, we discover an additional level of regulation in which the mechanically exposed VBS binds vinculin significantly more tightly than the isolated VBS alone. Molecular dynamics simulations reveal the basis of this new regulatory mechanism, identifying a sensitive force-dependent change in the conformation of an exposed VBS that modulates binding. Together, these results provide a comprehensive understanding of how the interplay between force and autoinhibition provides exquisite complexity within this major mechanosensing axis.

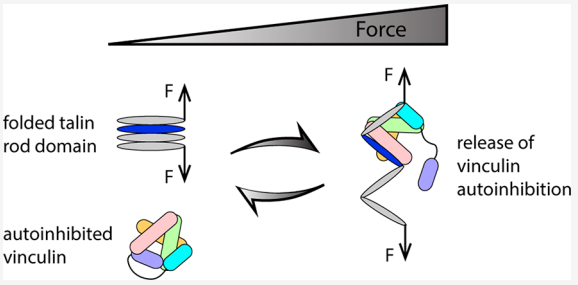

INTRODUCTION

Integrin-mediated adhesions are multicomponent molecular complexes that support the physical connection between cells and the extracellular matrix (ECM). At the core of these structures are the transmembrane integrins, α- and β-heterodimers that bind ECM proteins through their large extracellular domains and are connected to the intracellular actin cytoskeleton via adapter proteins such as talin[1] and vinculin.[2−4] Integrin adhesions are required for cells to sense the rigidity of their microenvironment, which is important in a variety of processes including tissue formation, maintenance, and repair.[5,6] Hence, understanding the fundamental mechanisms by which integrin adhesions sense and integrate mechanical signals is of crucial importance.

Talin plays a central role in integrin function and mechanosensing. By binding to β-integrin tails through its N-terminal four-point-one, ezrin, radixin, moesin (FERM) domain, talin initiates inside-out integrin activation,[7,8] while its large C-terminal rod domain supports the connection between integrins and F-actin.[9] When talin binds to integrins at one end and to F-actin at the other, it is mechanically stretched due to actomyosin contraction.[10−13] Previous studies have revealed that talin responds to external forces by changing conformation, which in turn affects interactions with its binding partners including vinculin.[14−20]

Vinculin, a 116 kDa cytoplasmic protein, has emerged as a key regulator of integrin adhesions.[4] It acts in part by cross-linking integrin−talin complexes to the actin cytoskeleton[4] and facilitates actin polymerization and nucleation.[21] Hence, vinculin plays a central role in cell adhesion formation, maturation, and turnover.[22] Full-length vinculin (FL-vinculin) is composed of five domains: D1, D2, D3, and D4, which together form the vinculin head that is connected via a proline-rich linker to the vinculin tail domain (Vt) (Figure 1). Interdomain interactions within the vinculin head organize the head into a pincer-like structure[23,24] (Figure 1). Vinculin binds to the 11 vinculin binding sites (VBSs) in the talin rod via its D1 domain, to F-actin through Vt, and to numerous other signaling proteins via interactions with various domains.[2,3,25,26]

Recent studies converge toward a model whereby talin may initially interact with vinculin in a force-independent regime,[27−30] leading to partial relief of autoinhibition, yet how these force-independent complexes transition into high-affinity mechanical linkages is not fully understood. High-

Received: June 18, 2021
Published: August 31, 2021

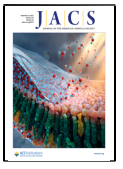

https://doi.org/10.1021/jacs.1c06223
J. Am. Chem. Soc. 2021, 143, 14726−14737

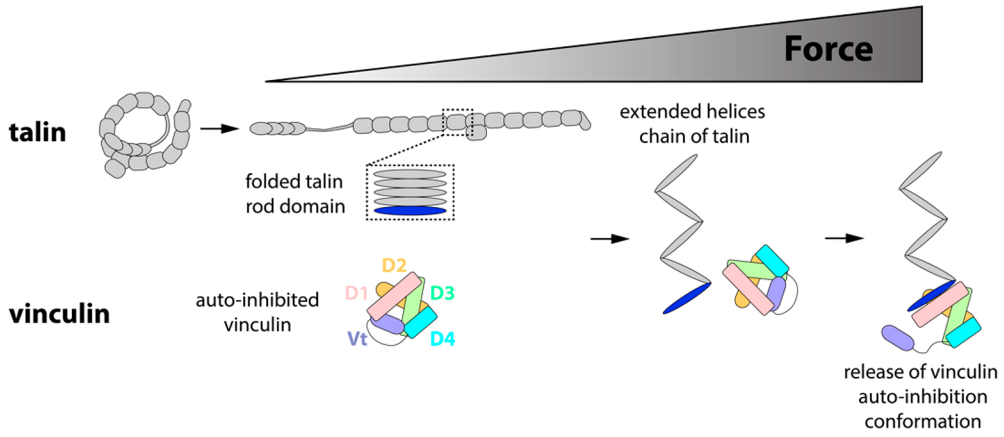

Figure 1. Schematic of the force-dependent vinculin activation by talin. In the absence of force, both the VBS (blue) in talin rod domains and FL-vinculin are autoinhibited. Force is needed to expose the VBS in the talin rod domain by unfolding the α-helix bundle. The mechanically exposed VBS can bind to the D1 domain (pink) and compete off the tail, Vt, which releases the autoinhibitory conformation.

affinity vinculin binding to talin requires exposure of the VBSs buried in the α-helical bundles in the talin rod domains.[14−16,31] Recent studies have revealed that forces within the physiological range, on the order of several piconewtons (pN), can fully expose the cryptic VBSs in talin and enable high-affinity vinculin D1 binding.[14−16] While previous studies have shown that isolated talin VBSs bind vinculin with dissociation constants over a range of 70−500 nM,[32] which could activate vinculin binding to actin filaments,[29] it remains unclear how mechanically exposed VBSs in the context of unfolded rod domains might interact with vinculin. In contrast to an isolated VBS, which exists in a force-free environment, the mechanically exposed VBSs in talin are under forces of several pN,[12,13,16] which may alter the conformation of the VBS, significantly impacting on the binding affinity[33] and kinetics.[34] Hence, further studies on the force-dependent conformations of VBSs under a few pN forces and the resulting effects on the vinculin−talin VBS interaction may provide insight into this important linkage.

A further layer of regulation arises from the fact that vinculin is also autoinhibited, and in the absence of other factors, vinculin adopts a compact globular conformation, in which the vinculin head interacts with the vinculin tail, suppressing its interactions with most of its binding partners (Figure 1). As the vinculin head binds to its tail with high affinity in vitro,[35,36] this autoinhibitory interaction is thought to be strong. Several models have been proposed to explain the vinculin activation process at cell adhesions. The widely accepted combinatorial model proposes that at least two binding partners are required to associate with the vinculin head and tail simultaneously to overcome the strong head−tail interaction.[23,37] However, based on the high-affinity interaction between vinculin D1 and the isolated talin VBS, the possibility of a single ligand activation model cannot be excluded. Since the vinculin−talin and vinculin autoinhibitory associations are mutually exclusive, the D1−VBS interaction may provide sufficient energy to compete off Vt from D1.[32,38,39] In addition, the crystal structure of autoinhibited vinculin shows that autoinhibition is mediated by a number of head−tail interactions, with the D1−Vt interaction being the predominant interaction. As such, disruption of the D1−Vt interaction by a talin VBS may destabilize the whole head−Vt interaction, driving a conformational change to a more extended activated conformation.[32]

Another important facet of the dynamics of these linkages is their lifetime. The talin-mediated force-transmission supramolecular linkages have an average lifetime on the order of minutes,[40] although a significant population of talin is immobile in focal adhesions[41] and at muscle attachment sites.[42] Therefore, the binding of vinculin to talin in cells happens within a limited time window. When talking about the head−tail autoinhibition of vinculin, one should consider whether such autoinhibition can significantly suppress the binding over this physiologically relevant time scale. After binding to talin's mechanically exposed VBSs, vinculin mediates a cascade of downstream biochemical events through interactions with a plethora of cytoskeletal and signaling proteins.[2,3,25,26] It is reasonable to believe that the longer the activated vinculin is associated with talin, the more persistent the vinculin-mediated mechanotransduction. Hence, the information on the lifetime of vinculin bound to talin under force is important but has not been investigated in previous studies.

In this study, we show that FL-vinculin can bind to a mechanically exposed talin VBS in R6 at ∼10 nM concentrations, much lower than the dissociation constants measured for isolated VBSs that are not under force.[32] Molecular dynamics (MD) simulation on isolated VBS reveals a propensity for the VBS helix to collapse into a compact hairpin-like arrangement in the absence of tensile force, which autoinhibits the VBS but can be released by physiological forces. The kinetics of the interaction between vinculin and the mechanically exposed VBS is characterized with a fast association rate k_{on} on the order of 10^6 $M^{-1}s^{-1}$ and a dissociation rate k_{off} on the order of 10^{-2} s^{-1}. In addition, by comparing the results with those obtained from vinculin D1, the vinculin head, and a vinculin T12 mutant with a weaker autoinhibitory head−tail interaction, we determine the influence of interdomain interactions within vinculin on the kinetics and affinity of the force-dependent vinculin−talin interaction.

RESULTS

A Force-Jump Cycle Assay to Quantitate Vinculin−Talin Complexation at the Single-Molecule Level. The interactions between the vinculin D1 domain and VBS-bearing talin, α-catenin, and α-actinin domains have been extensively studied.[14−16,43,44] In contrast, relatively little is known about

https://doi.org/10.1021/jacs.1c06223
J. Am. Chem. Soc. 2021, 143, 14726−14737

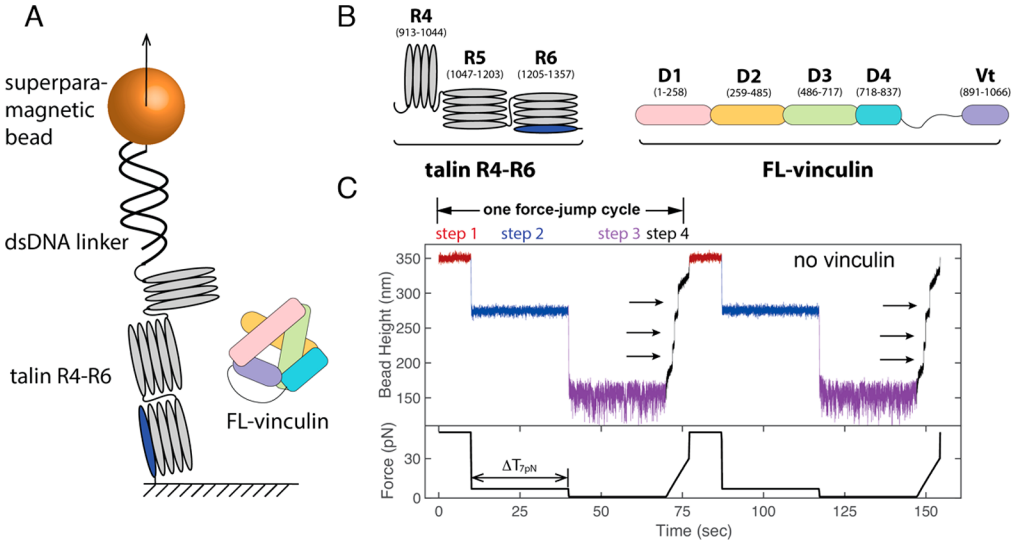

Figure 2. Force-jump cycle to detect and quantify vinculin binding. (A) Schematic of the talin R4−R6 domains tethered between a glass surface and a superparamagnetic bead. A 572-bp DNA linker is added as a spacer. (B) Domain map of talin R4−R6 (left) and FL-vinculin (right). The cryptic VBS in R6 is shown in blue. (C) Force-jump cycle applied to the talin R4−R6 domains in the absence of vinculin. Black arrows indicate the three discrete unfolding steps corresponding to R4−R6 domains (bottom: the experimental time trace of force change).

the force-dependent binding of FL-vinculin to these VBS-bearing mechanosensing proteins. In this study, we wanted to study binding of FL-vinculin to a well-characterized mechanosensitive system, and we chose talin domains R4−R6, which contain three α-helical bundles and a single VBS buried in R6 (helix 27) (Figure 2A,B). Talin R4−R6 were tethered between a glass surface and a superparamagnetic bead, which enabled force to be exerted onto the domains (Figure 2A).

To detect and quantify binding of FL-vinculin to mechanically unfolded R4−R6, we implemented a force-jump cycle approach (Figure 2C). Each force-jump cycle included the following steps: (1) a vinculin displacement step: the single-molecule construct was held at 50 ± 5 pN for 10 s to ensure displacement of any bound vinculin within seconds with 100% probability;[16] (2) a vinculin binding step: force-jump to a vinculin-binding force of 7 ± 0.7 pN for a certain time interval, ΔT_{7pN}, to allow vinculin binding to the mechanically exposed VBS; (3) a talin refolding step: force-jump to a domain-folding force of 1 ± 0.1 pN for 30 s to allow all domains to refold with 100% probability unless vinculin remains bound to the VBS, preventing refolding of R6;[16] and (4) binding detection step: force was increased from 1 ± 0.1 pN to 30 ± 3 pN at a loading rate of 4 ± 0.4 pN/s, during which all the domains unfold. After this step, force was jumped back to 50 ± 5 pN for the next vinculin displacement step, which completes one force cycle.

A vinculin-binding force of ∼7 pN was chosen to detect the binding of vinculin to mechanically exposed VBS, because it lies within the physiological range of forces (5−12 pN) applied to talin in cells.[12,16] In addition, at this force, refolding has never been observed over a long time scale (>400 s),[16] which ensured that the VBS was always exposed for binding. At the domain-folding force of ∼1 pN, in the absence of other factors, all talin rod domains fold almost immediately. In step 4 for the binding detection, if no vinculin was bound, then three unfolding events would be observed, as seen in Figure 2C. However, if a domain remains unfolded after 30 s, this can be attributed to vinculin binding to the VBS, preventing refolding of the VBS-containing R6 domain. Therefore, this assay enables us to monitor whether a vinculin molecule is bound to our talin molecule; if R6 is not able to refold in step 3 due to vinculin remaining bound, only two unfolding events from R4 and R5 would be observed, indicating formation of a talin−vinculin complex.

Response of Talin R4−R6 to Cyclic Force Perturbation. Figure 2C shows a representative time trace of more than 10 independent tethers of bead height change during a force cycle in the absence of vinculin. At step 1 where the tether was held at 50 ± 5 pN, the bead height fluctuated around a constant average level of 350 nm (data shown in red). The following force-jump to 7 ± 0.7 pN resulted in a large abrupt height decrease to an average level of 274 nm (data shown in blue). The next force-jump to 1 ± 0.1 pN resulted in another abrupt height decrease to an average level of 151 nm (data shown in purple). During the subsequent force-increase scan from 1 ± 0.1 pN to 30 ± 3 pN (data shown in black), three unfolding steps were observed (black arrows), indicating full refolding of all three domains when the construct was held at 1 ± 0.1 pN in this force cycle. Here we note that the abrupt bead height changes during sudden large force jumps are contributed from both intrinsic molecular extension change and bead rotation due to torque rebalance after the force change.[45] In contrast, the stepwise bead height changes during force-increase scans represent molecular extension changes. This is because the force change before and after the steps are less than 0.04 pN; hence the torque remains balanced and therefore the bead rotation is negligible.[45]

Vinculin Binds to Mechanically Unfolded Talin. Repeating the force cycle in the presence of 10 nM FL-vinculin revealed only two unfolding events (indicated by black arrows) at the binding detection step in the first force-jump cycle (Figure 3A) with ΔT_{7pN} = 30 s. This indicates that one domain did not refold at step 3 when the construct was held at 1 ± 0.1 pN for 30 s. Since the failure of the domain to refold was dependent on the presence of FL-vinculin, it was attributed to the vinculin-bound R6. In cycle 2, three unfolding steps were observed, indicating no vinculin was bound to the

https://doi.org/10.1021/jacs.1c06223
J. Am. Chem. Soc. 2021, 143, 14726−14737

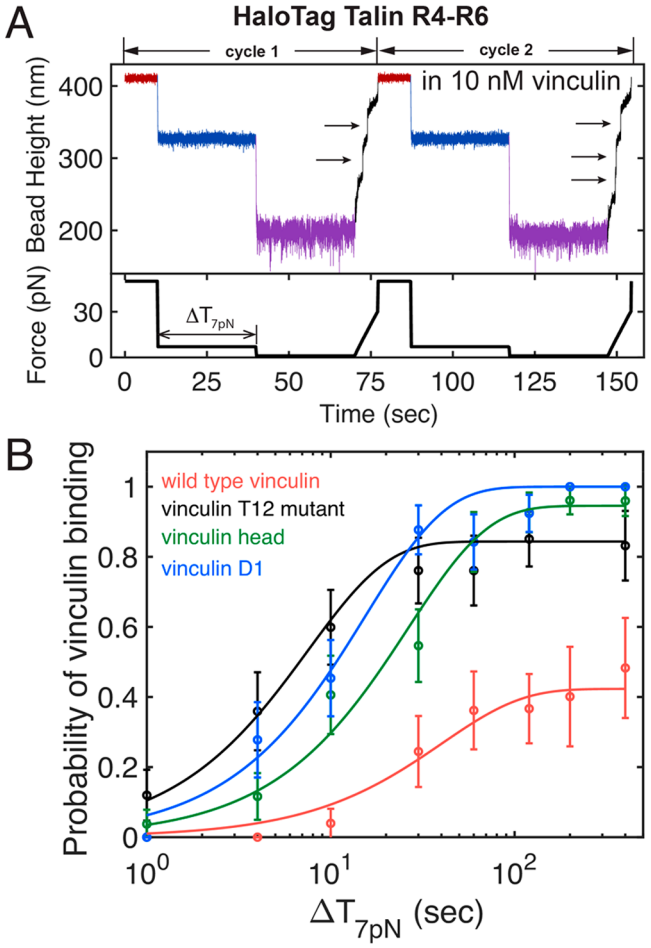

Figure 3. Full-length vinculin binds to mechanically exposed VBS in talin with nM affinity. (A) Representative force-jump cycles applied to detect and quantify vinculin binding. (B) Time evolution of binding probability for wild-type vinculin (red), T12 mutant (black), vinculin head (D1−D4, green), and vinculin D1 (blue). The evolution for vinculin binding probability was taken at ΔT_{7pN} = 1, 4, 10, 30, 60, 120, 200, and 400 s.

VBS in the vinculin-binding step. The probability of having a FL-vinculin bound during any given cycle provides important information on the binding affinity of the interaction.

The fact that vinculin binding was observed in these experiments indicates that mechanical exposure of the VBS in R6 is sufficient for FL-vinculin binding at nM concentrations, suggesting that the autoinhibitory head−tail interaction of vinculin is not strong enough to suppress vinculin binding to a mechanically exposed VBS.

Quantification of Vinculin Binding to a Mechanically Exposed VBS. We next sought to quantify the interaction between talin and vinculin by determining the binding kinetics and affinity. To do this, we implemented the force-jump cycle (Figure 2C) to obtain the probability of FL-vinculin binding to the mechanically exposed VBS in talin R6 at 7 ± 0.7 pN with different holding times ΔT_{7pN}. At each ΔT_{7pN}, the binding probability was determined by $\frac{N_b}{N}$ where $N \geq 15$ is the total force cycles obtained from multiple tethers and N_b is the number of cycles where vinculin binding was observed. Repeating the force cycle at different ΔT_{7pN}, we determined the time evolution of the binding probability $P(t)$ of FL-vinculin binding to the mechanically exposed VBS in talin R6.

In Figure 3B, the red data points show the probability of FL-vinculin binding to the mechanically exposed R6 VBS obtained at 10 nM FL-vinculin. Shown in red is the best-fit curve with $P(t) = \frac{ck_{on}}{ck_{on}+k_{off}}(1 - e^{-(ck_{on}+k_{off})t})$, where c, k_{on}, and k_{off} are vinculin concentration, association rate, and dissociation rate, respectively. The best-fit parameters are determined to be k_{on}= (1.0 ± 0.4) × 10^6 M^{-1} s^{-1} and k_{off} = (1.4 ± 0.9) × 10^{-2} s^{-1}, from which the dissociation constant was calculated to be $K_d = \frac{K_{off}}{K_{on}}$ = 12 ± 5 nM. We note that, to accurately determine the rate constants, it is important to choose ΔT_{7pN} that covers both non-equilibrium and equilibrium regimes (Supporting Information 1). The result indicates that FL-vinculin can directly bind to the mechanically exposed VBS in talin R6 with nM affinity. The standard error was calculated as the standard deviation of means based on bootstrap analysis with 200 repetitions (see Methods). The association rate is on the order of the diffusion-limited on-rate;[46] hence, the result strongly suggests that the FL-vinculin undergoes a highly dynamic fluctuation between the autoinhibited closed conformation and an open conformation accessible to the VBS.

Quantification of Vinculin T12 Mutant, Vinculin Head, and Vinculin D1 Binding to Mechanically Exposed VBS. Having established that FL-vinculin binds to a mechanically exposed VBS in talin, we next characterized the interaction in more detail using a series of well-established vinculin constructs. These included the "vinculin T12" mutant that has reduced autoinhibition due to a weaker head−tail interaction,[35] the entire vinculin head (D1−D4), and the VBS-binding domain of vinculin (D1), which is expected to bind talin with maximal affinity. Similar binding experiments were performed for each of these vinculin constructs to enable direct comparison with FL-vinculin (Figure 3B).

Vinculin T12 Mutant. The vinculin T12 mutant contains four mutated residues in the vinculin tail domain, Vt (D974A, K975A, R976A, and R978A).[35] Previous experiments have shown that the T12 mutant has a weaker head−tail interaction due to disruption of the D4−Vt interface, resulting in stronger binding to talin and enhanced focal adhesion formation and stabilization.[35] In our force-cycle experiments, 10 nM vinculin T12 (Figure 3B, black curve) bound to the mechanically exposed VBS in talin R4-R6 with the following best-fitting values, k_{on} = (1.1 ± 0.3) × 10^7 M^{-1} s^{-1} and k_{off} = (2.1 ± 1.1) × 10^{-2} s^{-1}. The dissociation constant was calculated to be K_d = 1.9 ± 0.5 nM. Compared to wild-type vinculin, T12 has a significantly faster association rate but a similar dissociation rate, resulting in a higher binding affinity indicated by a ∼6-fold lower dissociation constant.

Vinculin Head. The vinculin head comprises D1, D2, D3, and D4 domains that show extensive interdomain interactions, although the construct lacks the autoinhibitory Vt domain. Similar experiments performed in 10 nM vinculin head (Figure 3B, green curve) gave best-fitting values of k_{on}= (3.7 ± 0.9) × 10^6 M^{-1} s^{-1} and k_{off} = (2.2 ± 1.8) × 10^{-3} s^{-1}. The dissociation constant was calculated to be K_d = 0.6 ± 0.3 nM. The measured value of k_{off} is in good agreement with that reported from a previous fluorescence recovery after photobleaching (FRAP) measurement.[19]

Vinculin D1. Similar experiments with the vinculin D1 alone (Figure 3B, blue curve) determined a best-fitting value of k_{on} = (6.5 ± 1.6) × 10^6 M^{-1} s^{-1} and a near-zero k_{off} that cannot be accurately determined by fitting, due to ∼1 equilibrium

https://doi.org/10.1021/jacs.1c06223
J. Am. Chem. Soc. 2021, 143, 14726−14737

Table 1. Kinetic Rates and Affinity of Vinculin Binding to Mechanically Exposed VBS

	FL-vinculin	T12 vinculin	vinculin head	vinculin D1
k_{on} (M^{-1} s^{-1})	$(1.0 \pm 0.4) \times 10^{6}$	$(1.1 \pm 0.3) \times 10^{7}$	$(3.7 \pm 0.9) \times 10^{6}$	$(6.5 \pm 1.6) \times 10^{6}$
k_{off} (s^{-1})	$(1.4 \pm 0.9) \times 10^{-2}$	$(2.1 \pm 1.1) \times 10^{-2}$	$(2.2 \pm 1.8) \times 10^{-3}$	too low to be detectable
K_d (nM)	12 ± 5	1.9 ± 0.5	0.6 ± 0.3	not available

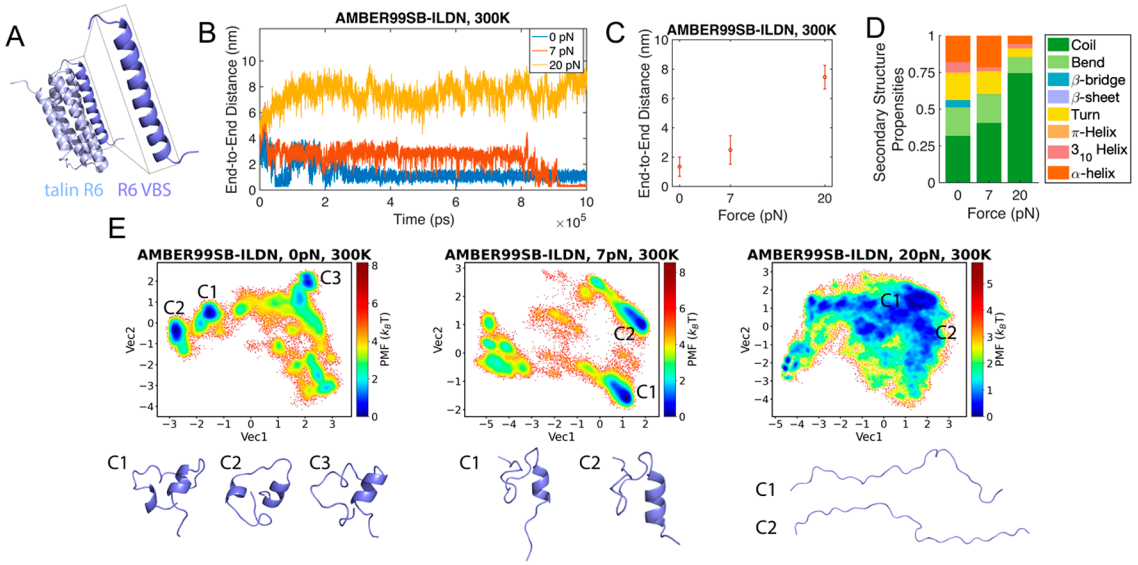

Figure 4. Force-dependent conformations of the talin R6 VBS. (A) Solution structure of the talin R6 domain (PDB 2l10). The inset shows the α-helical conformation of the R6 VBS used as the initial conformation. (B) Time traces of the end-to-end distance of the R6 VBS under different tensile forces using the AMBER99SB-ILDN force field at 300 K. (C) Mean and standard deviation of the end-to-end distance of the R6 VBS calculated from the time traces at 300 K using the AMBER99SB-ILDN force field. (D) Secondary structure propensities of the R6 VBS under different tensile forces using the AMBER99SB-ILDN force field at 300 K defined by DSSP. (E) Free energy landscape as a function of the first two dihedral principal components using the AMBER99SB-ILDN force field at 300 K at 0, 7, and 20 pN, with the representative conformations of identified local energy minima.

binding probability, $P_{eq} = \frac{ck_{on}}{ck_{on} + k_{off}}$, measured in our experiments. Together, these results suggest a much higher binding affinity for vinculin D1, which cannot be determined within our experimental time scale, than that of the vinculin head, FL-vinculin, and the T12 vinculin mutant.

The best-fitting values of k_{on} and k_{off} and the resulting K_d are summarized in Table 1. These results suggest that although all four forms of vinculin can bind the mechanically exposed VBS at nM concentrations, the binding affinity is the highest for D1 (K_d < 1 nM, Supporting Information 4) and the weakest for FL-vinculin. The dissociation rates for the FL-vinculin and the T12 mutant are similar; therefore, the increased affinity of T12 is mainly caused by a near 10-fold faster association rate compared to the wild-type vinculin. This suggests that the dynamic head−tail interaction within the wild-type vinculin reduces the time fraction of the open, accessible conformation. In contrast, the weaker head−tail interaction in T12 leads to a higher propensity to exist in a more accessible conformation, which is in line with a recent study reporting less energy is needed to shift from a closed to a semiopen state of T12 than that of wild-type vinculin.[47]

The association rates of vinculin head and D1 are faster than that of the FL-vinculin by several folds. In addition, their dissociation rates are ∼6-fold (for vinculin head) and much slower (for vinculin D1) than that of the FL-vinculin. Together, the faster association rates and slower dissociation rates result in the higher affinity of the vinculin head and D1 than that of the FL-vinculin.

Overall, these results reveal important differences between the binding of the four forms of vinculin to talin VBS. The most important is that, while the head−tail interaction of vinculin does not inhibit vinculin binding to mechanically exposed VBS, it significantly tunes the affinity mainly via modulating the rates of binding.

Force-Dependent Conformations of an Exposed Talin VBS Tune Its Affinity for Vinculin. A striking finding of our study is that the affinity of the talin−vinculin interaction observed under force is significantly higher than the bulk interactions of a talin VBS with FL-vinculin measured in solution (70−500 nM).[32] As the mechanically exposed VBSs have enhanced binding affinity relative to isolated VBSs in solution, it suggests that forces applied to a talin VBS strongly influence binding to vinculin. The talin−vinculin interaction involves the VBS binding as a helix to the D1 domain via a helix-addition mode of binding (illustrated in Supporting Figure 3A). In the folded talin rod domain, a VBS also adopts a helical conformation as part of the helical bundle. However, an exposed VBS, which is not bound to vinculin, has the potential to adopt various conformations besides the high affinity vinculin-binding helical form. Hence, we hypothesized that the isolated VBS may adopt thermodynamically stable auto-inhibited conformations that suppress its binding to vinculin D1. To evaluate the potential effect of force on VBS conformation, we performed 1 μs full-atom MD simulations on a VBS peptide with and without applied forces. The α-helical conformation obtained from the folded R6 domain

https://doi.org/10.1021/jacs.1c06223
J. Am. Chem. Soc. 2021, 143, 14726−14737

structure (PDB 2l10[31]) was used as the initial VBS conformation in the simulations (Figure 4A).

Simulations were performed on the R6 VBS by itself in a 150 mM NaCl solution starting from the initial α-helical conformation up to 1 μs under the AMBER99SB-ILDN[48] force field, at a temperature of 300 K (see Methods). The time traces of the end-to-end distance of the R6 VBS show significant dependence on the applied force (Figure 4B). In the absence of force, the end-to-end distance collapsed from the initial value (~4.1 nm) of the helical conformation to ~1.0 nm after 200 ns of simulation and remained in the compact conformation throughout the rest of the simulation. At 7 pN, the VBS assumed overall more extended conformations and larger extension fluctuations. At 20 pN, the end-to-end distance evolved from the initial value to a larger value (~8.4 nm), indicating transition to conformations that are more extended than the original helical conformation. Consistently, the average extension of R6 VBS monotonically increases as the applied force increases (Figure 4C). Together, the results reveal that forces in the physiological range strongly modulate the conformations and the extension of a VBS. It is likely that all exposed talin helices exhibit similar force-dependent conformational changes. Indeed, similar results were obtained from another talin VBS in R10, VBS3 (Supporting Information 3).

To obtain information on the predominant conformations at each force, we performed the dihedral principal component analysis (dPCA)[49] and used the first two principal component axes to recast the simulation data (see Methods). Figure 4E shows the free energy landscape of the R6 VBS as a function of the first two dihedral principal components of the 1 μs MD simulation in the absence of force, as well as at forces of 7 and 20 pN at 300 K using the AMBER99SB-ILDN force field, and a few representative predominant snapshots of conformations identified by dPCA at each force. At 0 pN, the free energy landscape represents multiple local energy minima and the corresponding R6 VBS conformations all exhibit compact hairpin-like structures. The 20 lowest energy structures of the R6 VBS, aligned on the first helical segment (residues 1330–1336) (Supporting Information 2), illustrates that the collapsed state is only partially ordered and has conformational heterogeneity rather than a single low-energy folded state. The NMR spectrum of the R6 VBS (Supporting Information 2) supports this assessment, as the lack of dispersion and relative broadness of the peaks is indicative of a peptide with some transient structural features but conformational heterogeneity. At 7 pN, the predominant conformations of the R6 VBS peptide become a mixture of helical and disordered regions. At 20 pN, the R6 VBS exists predominantly as a disordered, extended peptide. Figure 4D summarizes the amino acid secondary structure propensity in 1 μs MD simulations at different forces determined by the Dictionary of Protein Secondary Structure (DSSP) algorithm.[50] Similar results were also obtained from the VBS in R10 (Supporting Information 3).

Together, the simulations suggest that the conformation of an isolated talin VBS is very sensitive to the force applied over a physiological range. Interestingly, in the absence of forces, an isolated VBS has the propensity to collapse into energetically favorable hairpin-like conformations that not only drastically deform from the original α-helical conformation but also bury several critical residues that mediate the interaction with vinculin D1. This compact form is likely to be a previously unrecognized, autoinhibited conformation that binds D1 with reduced affinity. In addition, at too large a force (e.g., 20 pN), a VBS becomes a completely disordered peptide. At the physiologically relevant forces of a few pN such as 7 pN, a VBS is a dynamic mixture of helical and disordered regions which is expected to enhance binding to D1 compared with the collapsed hairpin-like conformations in the absence of force or the completely disordered peptide conformation at large forces, >20 pN. Consistent with this picture, the dissociation constant between isolated R6 VBS (helix 27) and vinculin D1 was determined to be 320 ± 130 nM using a fluorescence polarization assay (Supporting Information 4), which is orders of magnitude larger than that between mechanically stretched R6 VBS and vinculin D1. As further validation of this enhanced binding affinity of a VBS under force compared to an isolated VBS, we find that micromolar concentrations of isolated R6 VBS are required to inhibit vinculin D1 binding to a mechanically stretched R6 VBS (Supporting Information 4).

On the basis of the insights provided from the MD simulations, we developed a simple model to understand the force-dependent binding affinity between an isolated talin VBS and the VBS-binding D1 domain in vinculin. In this model, three structural states of the VBS are considered (Figure 5A): the α-helical conformation that binds D1 with the highest affinity (state "off, 2"), an autoinhibited hairpin-like conformation (state "off, 1"), and a disordered peptide conformation that does not bind D1 (state "off, 3"). Besides

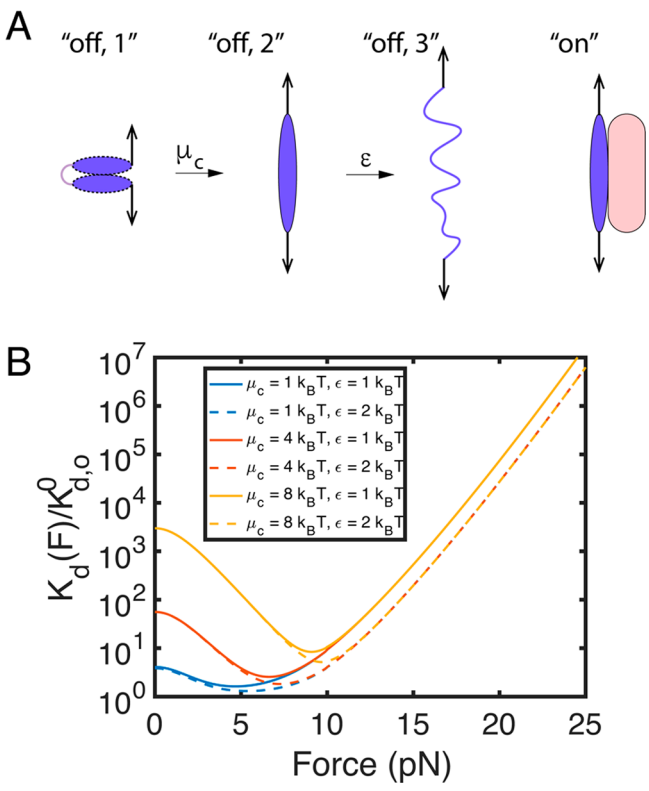

Figure 5. Force-dependency of the VBS conformation and its interaction with vinculin D1. (A) Schematic of four states of an isolated VBS, three unbound, "off" states, and the vinculin D1 bound "on" state. The pink rounded rectangle represents vinculin D1, which binds to the helical "on" conformation. (B) Fold change in the force-dependent binding constant, $K_d(F)$, of the VBS–D1 interaction (eq 1). Maximal binding affinity is seen in the trough of the curve at 5–11 pN dependent on the value of μ_c and ε.

https://doi.org/10.1021/jacs.1c06223
J. Am. Chem. Soc. 2021, 143, 14726–14737

the three "off" states of VBS unbound by D1, a fourth state where the VBS is bound to D1 (state "on") exists. On the basis of these four states, we derived a force-dependent dissociation constant of the VBS−D1 interaction as

$$K_d(F) = K_d^0(1 + e^{\beta\mu_c}e^{-\beta\Delta\phi_{1,2}(F)} + e^{-\beta\varepsilon}e^{-\beta\Delta\phi_{3,2}(F)}) \quad (1)$$

where $\beta = \frac{1}{k_B T}$. K_d^0 denotes the dissociation constant of the original α-helical conformation of VBS binding to D1 in the absence of force. μ_c is the autoinhibitory free energy stored in the ensemble of hairpin-like conformations, which is the free energy difference between the original α-helical conformation and the hairpin-like conformations. ε is the free energy difference between the ensemble of the unstructured peptide conformation and the α-helical conformation of the VBS. The value of ε tunes the probabilities of the α-helical conformation and the unstructured peptide conformations, which can be roughly understood as the stability of the α-helical conformation of the VBS. $\Delta\phi_{1,2}(F)$ is the force-induced conformational free energy difference between the "off, 1" and "off, 2" states, and similarly $\Delta\phi_{3,2}(F)$ is the force-induced conformational free energy difference between the "off, 3" and "off, 2" states. These force-induced conformational free energy differences can be calculated based on the different force−extension curves of the corresponding structural states i and j, $\Delta\phi_{i,j}(F) = -\int_0^F (x_i(f) - x_j(f))\,df$, where $x_i(f)$ is the force−extension curve of the conformation state "off, i". Details of the general physics behind the derivation can be found in our recent publication,[33] and the calculation for this particular case is provided in the Supporting Information (Supporting Information 5).

Figure 5B shows predicted K_d relative to K_d^0 for the VBS binding to the vinculin D1 as a function of force applied to the VBS (eq 1). As shown, with a reasonable assumption of k_BT level of the autoinhibition energy of μ_c in the hairpin-like structure, the equation predicts that forces of a few pN would significantly increase the binding affinity, which sensitively depends on the level of autoinhibition energy stored in the hairpin-like conformations. Furthermore, the force-dependent binding constant has maximal affinity (the trough on the curves in Figure 5B), which is determined by the stability of the VBS helix, as such helix stability further tunes the talin−vinculin interactions. As a result, further complexity and nuance are added to the talin−vinculin interactions, as even at the level of an exposed VBS the affinity between a VBS helix and vinculin is dynamically regulated by mechanical forces.

DISCUSSION

The interplay between talin and vinculin dictates mechanotransduction pathways downstream of integrins. A remarkable aspect of the interactions between these two proteins is its complexity. Both talin and vinculin adopt autoinhibited states, and once activated, the lifetimes of their association are largely defined by the mechanical conditions of the system and the history of prior forces that have acted on the linkages. In this study, we investigated the interaction between autoinhibited vinculin and talin, by using a three-domain talin construct, R4−R6, that contains a single cryptic VBS in R6. Strikingly, these two proteins do not interact in the absence of force, but mechanical exposure of the VBS in R6 is sufficient for binding to autoinhibited vinculin, revealing that force applied to talin alone is sufficient to activate high-affinity binding of vinculin in the absence of other factors. Furthermore, we identify an additional layer of regulation whereby the affinity of an exposed VBS for vinculin is fine-tuned by force-dependent changes in the conformation of the VBS helix itself. Steered full-atom molecular dynamics simulation reveals that a VBS peptide can adopt an autoinhibited stable hairpin-like conformation, which can be unfurled at physiological ranges of force. We reason that force may release the autoinhibited hairpin-like conformation of the VBS, enhancing its affinity for vinculin.

Autoinhibition of proteins involved in cell adhesion represents a major mechanism encoding mechanosensitivity[51] and enabling force-dependent binding constants.[33] Full-length talin and vinculin are both regulated by autoinhibition,[23,24,52,53] and a recent study by Atherton et al. using a mitochondrial targeting assay showed that the two autoinhibited proteins do not interact.[27] Release of the autoinhibition of either of the proteins led to their association in a force-independent manner. In the same study,[27] talin null cells coexpressing full-length vinculin and full-length talin under tension-released condition only formed small peripheral adhesions. Activation of either protein via mutagenesis was shown to be sufficient to enable their colocalization in focal adhesions under the condition where the actomyosin cytoskeleton contraction was suppressed using blebbistatin. However, the affinity of such force-independent association between talin and vinculin could be significantly weaker than that when VBSs in talin are mechanically exposed. Indeed, in the same study the authors showed that actomyosin contraction was needed for full maturation of focal adhesion. Similar force-independent talin−vinculin interactions have been proposed previously by Han et al. via a weak talin R8−vinculin D1 interaction[30] indicated by a dissociation constant on the order of μM range.[54] Such force-independent precomplexation between talin and vinculin was shown to be required for efficient adhesion maturation. The presence of phosphoinositides at the membrane has also been shown to be able to activate talin and enable force-independent interactions with vinculin.[28] Here, we show that full-length vinculin can bind to the mechanically exposed VBS in talin R6 with nM affinity, indicating that mechanical activation of talin is sufficient to trigger high-affinity binding to full-length vinculin. Together, these results highlight the cascade of activation steps that ultimately lead to the interactions between these two proteins. It is likely that there are multiple diverse pathways and mechanisms that can bring talin and vinculin together prior to tension and the assembly of mechanical linkages.

Binding of vinculin to a mechanically exposed talin VBS is fast, with an association rate of $\sim 10^6$ M^{-1} s^{-1}, close to the typical diffusion-limited association rate.[46] This is surprising, since vinculin was thought to adopt a strongly autoinhibited closed conformation due to the Vt−D1 interaction.[23,24,35] The fast association rate observed in our experiment strongly suggests that the autoinhibitory Vt−D1 interaction does not significantly slow down the binding of vinculin to a mechanically exposed talin VBS. Therefore, we propose that vinculin must undergo spontaneous rapid dynamic fluctuation between the open and closed states, making the vinculin D1 domain accessible for rapid binding to a talin VBS.

Force-Independent Talin−Vinculin Interactions Enhance the Association Rate. An unexpected finding of this work is that the vinculin T12 mutant has the fastest association rate of all of the vinculin constructs tested. The vinculin D1

https://doi.org/10.1021/jacs.1c06223
J. Am. Chem. Soc. 2021, 143, 14726−14737

domain interacts with the mechanically exposed VBS with an association rate of $(6.5 \pm 1.6) \times 10^6$ M^{-1} s^{-1}, which is faster than that of the entire vinculin head (D1−D4 domains) or wild-type vinculin, but slightly slower than the T12 mutant. It is surprising that T12 binds the exposed VBS with a rate faster than either D1 or the head, as neither of them contains the autoinhibitory Vt domain. We therefore expected that binding of constructs lacking Vt would be faster than both the wild-type vinculin and the T12 mutant. One possible explanation for this result is that the Vt domain and/or the preceding linker region might make some form of nonspecific interactions with the unfolded talin domains. Unfolded talin rod domains expose a lot of hydrophobic side chains, and the helical propensity and hydrogen bond forming tendency of these exposed sequences mean such nonspecific interactions are quite possible. Such nonspecific interactions would increase the effective local concentration of vinculin, promoting a fast binding rate of the vinculin D1 domain in the T12 mutant to the VBS. The Vt domain and the linker may therefore mediate precomplexation of FL-vinculin with partially exposed VBS-containing sites prior to canonical VBS−D1 engagement. This interaction would accelerate binding to the VBS once it is mechanically exposed.

It is also interesting to note that the equilibrium binding probability of the vinculin D1 domain to the mechanically exposed R6 VBS reached ∼1 in 10 nM vinculin D1, suggesting an ultraslow dissociation rate that could not be quantified in our assay. The dissociation rate of the head was about 6-fold and 10-fold slower than that of the wild-type vinculin and the vinculin T12 mutant, respectively. Therefore, compared with the wild-type vinculin and the T12 mutant, the D1 and head domains have the highest affinity mainly due to their slower dissociation rate. This high affinity of D1 locks talin in an unfolded conformation,[15] and expression of vinculin D1 in cells leads to a loss of adhesion dynamics[11,55] and lethality in flies.[56] Although the vinculin head−tail interaction is insufficient to inhibit vinculin binding to a mechanically exposed talin VBS, our results reveal that it significantly tunes the affinity and binding rates between vinculin and the VBS. The T12 mutant with weakened head−tail interaction binds the VBS with an affinity 6-fold higher compared to the wild-type vinculin, suggesting that the head−tail interaction suppresses the binding of vinculin to a talin VBS. Previous work has identified that phosphorylation of vinculin, including at Y100 and Y1605 by Src kinases, can stabilize the open state.[57,58] While our data show that stretching talin alone is sufficient to activate vinculin, phosphorylation of these sites would stabilize the open conformation of vinculin, extending the lifetimes of these mechanical linkages.

In this scenario, the master switch for both talin binding to vinculin and for vinculin activation is the mechanical unfolding of talin rod domains. Thus, we conclude that talin is the mechanical switch for talin/vinculin-dependent mechanotransduction. Consistently, previous studies have revealed that talin/vinculin-dependent focal adhesion development and maturation require a sufficiently rigid substrate,[59] on which talin is expected to experience considerable mechanical stretching. In addition, earlier work shows that applying external force to focal adhesion sites results in increased recruitment of vinculin to the perturbed sites.[60] These previous results are consistent with the talin mechanical switch model.

Identification of an Additional Layer of Talin Autoinhibition. Talin is regulated by many layers of autoinhibition,[61] from the fully closed form in the cytosol, which, upon relief of this head−tail autoinhibition, can open up to reveal the linear arrangement of helical bundles. These bundles are autoinhibited with respect to vinculin binding, as they contain cryptic VBSs within the bundles themselves. At physiological levels of stretching, e.g., 5−15 pN talin, bundles unfold, exposing the previously cryptic VBS, a well-characterized major mechanosensitive event.[15,16] These domains remain unfolded even when the force is reduced to just a few pN, providing them with a mechanical memory.[16] Here we define an additional, previously unrecognized, layer of autoinhibition on talin, at the level of the individual VBS. Our MD simulations and the enhanced affinity for a VBS under force suggest that forces over a few pN range increase the binding affinity by suppressing the VBS from adopting a low-affinity, hairpin-like conformation. This provides an explanation for the higher binding affinity quantified in our single-molecule experiments, where the VBS is under ∼7 pN forces (Table 1), compared with that from bulk measurement, where the VBS is not under force.[32] Similarly, the dissociation constant between isolated R6 VBS and vinculin D1 was found to be about 2 orders of magnitude larger than that between mechanically stretched R6 VBS and vinculin D1 (Supporting Information 4). We note that mechanically exposed talin VBSs in live cells are under a similar level of tensile forces.[12,13] Further increases in force on a VBS reduce its binding affinity for vinculin by decreasing the α-helical fraction of the VBS.[15] Therefore, forces biphasically tune the binding affinity of the exposed VBSs for vinculin. This changing binding affinity as forces on talin fluctuate means that the affinity for vinculin is dynamically tuned, even for an exposed VBS. Due to all these modulators, the force-dependent interactions of even a single VBS with vinculin are complex, and talin has 11 VBSs.

Identification of an Additional Layer of Vinculin Autoinhibition. One intriguing finding of this work is that D1 binds faster and more tightly to an exposed VBS than the vinculin head, which suggests that the interdomain interactions within the vinculin head suppress vinculin binding to talin. This raises the possibility of an additional layer of vinculin autoinhibition whereby the D1−VBS interaction is hindered by the other head domains, slowing down the binding rate compared to D1 alone. As vinculin also makes a mechanical linkage when it cross-links talin to actin, it too will experience mechanical forces acting on it, and these forces, exerted only when vinculin forms a mechanical linkage, will extend vinculin. It is possible that the interdomain interactions in the vinculin head can be released by force-dependent changes in the conformation of the head, enhancing talin binding. Such a scenario would explain our data here, and if this is the case, it would suggest that the stability of vinculin bound on talin might also be modulated by force, this time acting on vinculin. Future studies should investigate the effects of forces exerted on vinculin binding to an exposed VBS to confirm this layer of autoinhibition of the talin−vinculin and how force on vinculin modulates its affinity for talin.

Talin−Vinculin Complexes as a Way to Encode Mechanical Memory. In this study we have focused on the talin module R4−R6 that contains a single VBS in order to work with a simplified system, and we show that force on talin drives talin−vinculin complex formation. Complexation stabilizes the open conformations of the domains and thus alters the lifetimes of the active conformations. Further, stabilization of such interactions in vivo will occur when the

https://doi.org/10.1021/jacs.1c06223
J. Am. Chem. Soc. 2021, 143, 14726−14737

vinculin tail engages an actin filament,[37] which both stabilizes the open conformation of vinculin and increases the mechanical linkages on that integrin−talin−actin connection. In a cell, there is the opportunity for incredible diversity and complexity in these mechanical linkages based on the mechanical responses we have identified. Each adhesive structure contains many talin molecules,[62] each of which contains 13 rod domains.[31] The 13 rod domains of talin can be envisaged as binary switches with two states, folded "0" and unfolded "1", and can be converted between these states by changes in mechanical force.[16] Within 9 of the talin rod domains reside 11 VBSs, each of which can be exposed by mechanical force to bind vinculin. Therefore, just considering the interaction between vinculin and talin alone, the complexity of the mechanical linkages that can form is staggering. Further complexity emerges with the discovery that the talin switches can be modulated by post-translational modifications such as phosphorylation, altering their mechanical response.[63] It is possible that other enzymes may also modify the talin switches in response to signaling, altering the mechanical information stored in these linkages and the resulting signaling hubs that assemble.[18] The patterns of 1s and 0s in each talin molecule will be stabilized by vinculin binding to give persistent mechanical linkages, and the effect of future forces on the mechanical linkages will result in additional exposure of VBSs in other domains, explicitly dependent on the talin−vinculin complexes already present. This provides a basis for these mechanical linkages to exhibit mechanical memory as recently described in the MeshCODE theory[64] with information stored in the shape of these molecules and the cytoskeletal connections that form as a result.

CONCLUSIONS

In summary, we provide a comprehensive analysis of the complex interactions between full-length vinculin and a mechanically exposed VBS in talin, defining the fundamental mechanisms that regulate such interactions. In doing so we further expand our understanding of these crucial linkages that control mechanotransduction downstream of integrins.

METHODS

Protein Expression and Purification. All plasmids were expressed in *Escherichia coli* BL21(DE3) cultured in Luria−Bertani (LB) media. The stretchable talin R4−R6 fragment was expressed and purified as reported previously.[16] Briefly, the expressed protein was purified via the GST-tag, using glutathione Sepharose resin (GE Healthcare) before being eluted by TEV cleavage. The FL-vinculin and vinculin T12 mutant plasmid constructs were synthesized by GeneArt gene synthesis and cloned into an expression vector (pET-28b). The vinculin head and vinculin D1 were cloned into the pET-151 expression vector. The His-tagged vinculin proteins were purified through the His-tag followed by anion exchange using standard protocols.[65] Protein concentrations were determined using the respective extinction coefficients at 280 nm.

Single-Molecule Manipulation. An in house-made backscattered vertical magnetic tweezers was used in the single-molecule manipulation experiments with a spatial resolution of ∼1 nm and temporal resolution of ∼200 Hz.[45,66] Talin R4−R6 domains was tethered to the coverslip through its C-terminal HaloTag/ligand system, while its N-terminus was linked to a superparamagnetic bead through a 572-bp double-stranded DNA linker. This system was performed in a laminar flow channel. The extension change of the tethered protein was measured based on the height change of the superparamagnetic beads tethered to the protein under force.

The details of the force calibration and control for the single-molecule magnetic tweezers experiments have been described in previous papers.[45,66]

Determination of k_{on}, k_{off}, K_d, and Error Estimation. The binding kinetics involve the association and dissociation of binding, which are characterized by the association rate k_{on} and the dissociation rate k_{off}, respectively. Denoting P as the probability of the VBS in the unfolded talin R6 bound by vinculin, it satisfies the equation $\frac{dP}{dt} = ck_{on}(1 - P) - k_{off}P$, where c represents the vinculin concentration. With the well-controlled initial condition $P(0) = 0$, which refers to the assured unbound condition of talin R6 VBS at the starting point of step 2 (Figure 2C), the equation can be solved as $P(t) = \frac{ck_{on}}{ck_{on} + k_{off}}(1 - e^{-(ck_{on}+k_{off})t})$.

By implementing the force-jump cycles, the cycles with vinculin binding and those without vinculin binding at the vinculin-binding force (7 pN) can be recorded. At each time interval at 7 pN, ΔT_{7pN}, an array A comprising N elements of 0 or 1 was generated, where $N \geq 15$ is the total number of cycles from multiple independent tethers. Elements of "0" and "1" indicate the cycles where the VBS was "unbound" and "bound", respectively. In our experiments, the force cycles were performed at the following time intervals: ΔT_{7pN} = 1, 4, 10, 30, 60, 120, 200, 400 s.

After that, bootstrap analysis was performed for 200 repetitions to estimate the mean and the error of the fitted rates. Each bootstrap analysis randomly chooses N data points from the array A with replacement[67] and calculated the mean value of the N randomly selected data points, which is the probability of binding $P_i(\Delta T_{7pN})$, at each ΔT_{7pN}, where i = 1, ..., 200 refers to the ith bootstrap analysis. For each bootstrap analysis, the resulting $P_i(\Delta T_{7pN})$ was fitted with the function $P_i(\Delta T_{7pN}) = \frac{ck_{on,i}}{ck_{on,i} + k_{off,i}}(1 - e^{-(ck_{on,i}+k_{off,i})\Delta T_{7pN}})$, from which the best-fitting values of $k_{on,i}$ and $k_{off,i}$ were obtained. Based on the fitted values of association rate $k_{on,i}$ and dissociation rate $k_{off,i}$, the dissociation constant $K_{d,i}$ can thus be determined by $K_{d,i} = \frac{k_{off,i}}{k_{on,i}}$. Upon completion of a 200-repetition bootstrap (i.e., i was taken from 1 to 200), the mean values of the association rate k_{on}, dissociation rate k_{off}, and dissociation constant K_d were determined as the average over all $k_{on,i}$, $k_{off,i}$, and $K_{d,i}$, respectively. The standard errors associated with k_{on}, k_{off}, and K_d were determined as the standard deviations of $k_{on,i}$, $k_{off,i}$, and $K_{d,i}$, respectively.

Molecular Dynamics Simulation. The MD simulation was performed using GROMACS 2020.2.[68,69] The initial talin VBS structures were the R6 VBS (PASPNLKSQLAAAARAVTDS-INQLITMCTQQA) structure taken from the NMR structure of the talin R6 domain (PDB 2l10[31]) and the R10 VBS (YTKKELIE-SARKVSEKVSHVLAALQA) structure taken from the X-ray structure of the R10 VBS-human vinculin D1 complex (PDB 1rkc[38]), which both adopt the α-helical conformation. The simulations were performed under the AMBER99SB-ILDN force field[48] using the TIP3P[70] water model. The initial VBS molecule was immersed in a periodic cuboid water box filled with 0.15 M NaCl solution. A cutoff distance of 1 nm was applied to the Lennard-Jones interactions and short-range electrostatic interactions. Long-range electrostatic interactions were calculated using the particle-mesh Ewald method with a grid spacing of 0.16 nm and fourth-order interpolation.

A total of 500 steps of steepest descent energy minimization were performed for the simulation system to ensure a reasonable starting structure. Thereafter the energetically minimized system was subjected to a 100 ps NVT equilibration heating and stabilizing the system at 300 K, followed by a 100 ps NPT equilibration stabilizing the pressure of the system. Upon completion of the energy minimization and two-step equilibration, a 1 μs MD simulation was performed during which the system coordinates were stored every 10 ps for further analysis.

To apply constant force (7 and 20 pN) to the VBS molecule in the MD simulation, the N-terminal residue was fixed and the C-terminal residue was subjected to the corresponding constant force.

https://doi.org/10.1021/jacs.1c06223
J. Am. Chem. Soc. 2021, 143, 14726−14737

Dihedral Angle Principal Component Analysis and Free Energy Landscape. Principal component analysis is a dimensionality-reduction method used to identify and retain the most important degrees of freedom of a dynamic simulation system.[71,72] dPCA has been developed to use the sine- and cosine-transformed backbone dihedral angles as internal coordinates in the PCA of the MD simulations.[49]

In this work, 60 peptide backbone dihedral angles of the 32-aa R6 VBS peptide as well as 48 peptide backbone dihedral angles of the 26-aa R10 VBS peptide were used to perform the dPCA. Upon extraction of the dihedral angles from simulation trajectory and implementation of sine and cosine transformation of the dihedral angles, the covariance matrix can be calculated based on the sine and cosine variables obtained from the trajectory of dihedral angles. By diagonalizing the covariance matrix, eigenvectors Vec_i and eigenvalues λ_i can be obtained and organized in an eigenvalue-descending order, which means λ_1 represents the largest eigenvalue. Thereafter in this work, the first two eigenvectors Vec_1 and Vec_2 associated with the first two largest eigenvalues (i.e., the first two principal components) were chosen to recast the simulation data by projecting the data onto Vec_1 and Vec_2.

Subsequently, the free energy landscape along the first two principal components can be expressed by $\Delta G(Vec_1, Vec_2) = -k_B T \ln \frac{P(Vec_1, Vec_2)}{P_{max}}$, where k_B is the Boltzmann constant, T is the temperature, $P(Vec_1, Vec_2)$ refers to the probability distribution of the system around (Vec_1, Vec_2), and P_{max} is the maximum value of the probability distribution.

Protein Secondary Structure Assignments by Dictionary of Protein Secondary Structure. DSSP is an algorithm assigning secondary structure to the protein residues on the basis of hydrogen bond patterns.[50] The DSSP defines eight types of secondary structures: α-helix, 3_{10} helix, π-helix, hydrogen-bonded turn, β-sheet, β-bridge, bend, and coil. In this work, the secondary structures of VBS residues were analyzed by using the GROMACS do_dssp command with calling the dssp program.

Fluorescence Polarization Assay. A peptide corresponding to helix 27 of talin (residues 1324−1359) was synthesized by GLBiochem (China) TDPASPNLKSQLAAAARAVTDSINQLITMCTQQAPG. The peptide was coupled to a thiol-reactive fluorescein dye via the cysteine and stock solution made in phosphate-buffered saline (PBS; 137 mM NaCl, 27 mM KCl, 100 mM Na_2HPO_4, 18 mM KH_2PO_4, pH 7.4), 1 mM TCEP, and 0.05% Triton X-100. Excess dye was removed using a PD-10 desalting column (GE Healthcare, Chicago, IL, USA). The titration was performed in PBS using a constant 1 μM concentration of peptide with increasing concentration of protein; final volume 100 μL in a black 96-well plate. Fluorescent polarization measurements were recorded on a BMGLabTech CLARIOstar plate reader at room temperature and analyzed using GraphPad Prism. The details of the fitting function to determine the K_d value can be found in Supporting Information 4.

■ ASSOCIATED CONTENT

Supporting Information

The Supporting Information is available free of charge at https://pubs.acs.org/doi/10.1021/jacs.1c06223.

Requirement for the choice of ΔT_{7pN}; detailed analysis of the collapsed hairpin-like arrangement of the isolated R6 VBS; MD simulation on talin R10 VBS; direct measurement of the binding constant between unstretched R6 VBS and vinculin D1, as well as the competition assay between stretched and unstretched R6 VBS binding to vinculin D1; derivation of force-dependent binding affinity of D1−VBS interaction based on a four-state model; figures illustrating two regimes of FL-vinculin binding to unfolded talin R6; structural analysis of an isolated R6 VBS; MD simulation on isolated talin R10 VBS; fluorescence polarization measurement of binding constant between unstretched R6 VBS and vinculin D1, and competition assay between stretched and unstretched R6 VBS binding to vinculin D1; box providing the models and parameters of force−extension curves of R6 VBS used to predict the force-dependent binding constant (PDF)

■ AUTHOR INFORMATION

Corresponding Authors

Benjamin T. Goult − *School of Biosciences, University of Kent, Canterbury CT2 7NJ, U.K.*; orcid.org/0000-0002-3438-2807; Email: b.t.goult@kent.ac.uk

Jie Yan − *Department of Physics, National University of Singapore, Singapore 117546, Singapore; Mechanobiology Institute, National University of Singapore, Singapore 117411, Singapore*; orcid.org/0000-0002-8555-7291; Email: phyyj@nus.edu.sg

Authors

Yinan Wang − *Department of Physics, National University of Singapore, Singapore 117546, Singapore*; orcid.org/0000-0003-4111-6707

Mingxi Yao − *Department of Biomedical Engineering, Southern University of Science and Technology, Shenzhen, Guangdong 518055, China*

Karen B. Baker − *School of Biosciences, University of Kent, Canterbury CT2 7NJ, U.K.*

Rosemarie E. Gough − *School of Biosciences, University of Kent, Canterbury CT2 7NJ, U.K.*

Shimin Le − *Department of Physics, National University of Singapore, Singapore 117546, Singapore*; orcid.org/0000-0003-2359-1897

Complete contact information is available at: https://pubs.acs.org/10.1021/jacs.1c06223

Author Contributions

Y.W. carried out the single-molecule experiments and molecular dynamics simulations. Y.W., M.Y., and S.L. performed data analysis. Y.W., M.Y., K.B.B., R.E.G., and S.L. contributed to the design and expression of the protein constructs for single-molecule experiments. Y.W., J.Y., and B.T.G. interpreted the experimental and simulation data. J.Y. and B.T.G. supervised the research. Y.W., J.Y., and B.T.G. wrote the paper.

Notes

The authors declare no competing financial interest.

■ ACKNOWLEDGMENTS

We thank David Critchley for critical reading of the manuscript. J.Y. was funded by the Singapore Ministry of Education Academic Research Fund Tier 2 (MOE2019-T2-1-099) and the Ministry of Education under the Research Centres of Excellence program. B.T.G. was funded by BBSRC (BB/N007336/1 and BB/S007245/1). B.T.G. and J.Y. were funded by HFSP (RGP00001/2016).

■ REFERENCES

(1) Horwitz, A.; Duggan, K.; Buck, C.; Beckerle, M. C.; Burridge, K. Interaction of plasma membrane fibronectin receptor with talin—a transmembrane linkage. *Nature* **1986**, *320* (6062), 531−533.

(2) Burridge, K.; Mangeat, P. An interaction between vinculin and talin. *Nature* **1984**, *308* (5961), 744−746.
(3) Johnson, R. P.; Craig, S. W. F-actin binding site masked by the intramolecular association of vinculin head and tail domains. *Nature* **1995**, *373* (6511), 261−264.
(4) Humphries, J. D.; Wang, P.; Streuli, C.; Geiger, B.; Humphries, M. J.; Ballestrem, C. Vinculin controls focal adhesion formation by direct interactions with talin and actin. *J. Cell Biol.* **2007**, *179* (5), 1043−1057.
(5) Edelman, G. M. Cell adhesion molecules in the regulation of animal form and tissue pattern. *Annu. Rev. Cell Biol.* **1986**, *2* (1), 81−116.
(6) Mammoto, T.; Ingber, D. E. Mechanical control of tissue and organ development. *Development* **2010**, *137* (9), 1407−1420.
(7) Calderwood, D. A.; Zent, R.; Grant, R.; Rees, D. J. G.; Hynes, R. O.; Ginsberg, M. H. The talin head domain binds to integrin β subunit cytoplasmic tails and regulates integrin activation. *J. Biol. Chem.* **1999**, *274* (40), 28071−28074.
(8) Goult, B. T.; Bouaouina, M.; Elliott, P. R.; Bate, N.; Patel, B.; Gingras, A. R.; Grossmann, J. G.; Roberts, G. C.; Calderwood, D. A.; Critchley, D. R. Structure of a double ubiquitin-like domain in the talin head: a role in integrin activation. *EMBO J.* **2010**, *29* (6), 1069−1080.
(9) Giannone, G.; Jiang, G.; Sutton, D. H.; Critchley, D. R.; Sheetz, M. P. Talin1 is critical for force-dependent reinforcement of initial integrin−cytoskeleton bonds but not tyrosine kinase activation. *J. Cell Biol.* **2003**, *163* (2), 409−419.
(10) Kanchanawong, P.; Shtengel, G.; Pasapera, A. M.; Ramko, E. B.; Davidson, M. W.; Hess, H. F.; Waterman, C. M. Nanoscale architecture of integrin-based cell adhesions. *Nature* **2010**, *468* (7323), 580−584.
(11) Margadant, F.; Chew, L. L.; Hu, X.; Yu, H.; Bate, N.; Zhang, X.; Sheetz, M. Mechanotransduction in vivo by repeated talin stretch-relaxation events depends upon vinculin. *PLoS Biol.* **2011**, *9* (12), e1001223.
(12) Austen, K.; Ringer, P.; Mehlich, A.; Chrostek-Grashoff, A.; Kluger, C.; Klingner, C.; Sabass, B.; Zent, R.; Rief, M.; Grashoff, C. Extracellular rigidity sensing by talin isoform-specific mechanical linkages. *Nat. Cell Biol.* **2015**, *17* (12), 1597−1606.
(13) Kumar, A.; Ouyang, M.; Van den Dries, K.; McGhee, E. J.; Tanaka, K.; Anderson, M. D.; Groisman, A.; Goult, B. T.; Anderson, K. I.; Schwartz, M. A. Talin tension sensor reveals novel features of focal adhesion force transmission and mechanosensitivity. *J. Cell Biol.* **2016**, *213* (3), 371−383.
(14) Del Rio, A.; Perez-Jimenez, R.; Liu, R.; Roca-Cusachs, P.; Fernandez, J. M.; Sheetz, M. P. Stretching single talin rod molecules activates vinculin binding. *Science* **2009**, *323* (5914), 638−641.
(15) Yao, M.; Goult, B. T.; Chen, H.; Cong, P.; Sheetz, M. P.; Yan, J. Mechanical activation of vinculin binding to talin locks talin in an unfolded conformation. *Sci. Rep.* **2015**, *4* (1), 1−7.
(16) Yao, M.; Goult, B. T.; Klapholz, B.; Hu, X.; Toseland, C. P.; Guo, Y.; Cong, P.; Sheetz, M. P.; Yan, J. The mechanical response of talin. *Nat. Commun.* **2016**, *7* (1), 1−11.
(17) Hu, X.; Jing, C.; Xu, X.; Nakazawa, N.; Cornish, V. W.; Margadant, F. M.; Sheetz, M. P. Cooperative vinculin binding to talin mapped by time-resolved super resolution microscopy. *Nano Lett.* **2016**, *16* (7), 4062−4068.
(18) Goult, B. T.; Yan, J.; Schwartz, M. A. Talin as a mechanosensitive signaling hub. *J. Cell Biol.* **2018**, *217* (11), 3776−3784.
(19) Ciobanasu, C.; Faivre, B.; Le Clainche, C. Actomyosin-dependent formation of the mechanosensitive talin−vinculin complex reinforces actin anchoring. *Nat. Commun.* **2014**, *5* (1), 1−10.
(20) Vigouroux, C.; Henriot, V.; Le Clainche, C. Talin dissociates from RIAM and associates to vinculin sequentially in response to the actomyosin force. *Nat. Commun.* **2020**, *11* (1), 1−11.
(21) Wen, K.-K.; Rubenstein, P. A.; DeMali, K. A. Vinculin nucleates actin polymerization and modifies actin filament structure. *J. Biol. Chem.* **2009**, *284* (44), 30463−30473.
(22) Bays, J. L.; DeMali, K. A. Vinculin in cell−cell and cell−matrix adhesions. *Cell. Mol. Life Sci.* **2017**, *74* (16), 2999−3009.
(23) Bakolitsa, C.; Cohen, D. M.; Bankston, L. A.; Bobkov, A. A.; Cadwell, G. W.; Jennings, L.; Critchley, D. R.; Craig, S. W.; Liddington, R. C. Structural basis for vinculin activation at sites of cell adhesion. *Nature* **2004**, *430* (6999), 583−586.
(24) Borgon, R. A.; Vonrhein, C.; Bricogne, G.; Bois, P. R.; Izard, T. Crystal structure of human vinculin. *Structure* **2004**, *12* (7), 1189−1197.
(25) Brindle, N. P.; Holt, M. R.; Davies, J. E.; Price, C. J.; Critchley, D. R. The focal-adhesion vasodilator-stimulated phosphoprotein (VASP) binds to the proline-rich domain in vinculin. *Biochem. J.* **1996**, *318* (3), 753−757.
(26) DeMali, K. A.; Barlow, C. A.; Burridge, K. Recruitment of the Arp2/3 complex to vinculin: coupling membrane protrusion to matrix adhesion. *J. Cell Biol.* **2002**, *159* (5), 881−891.
(27) Atherton, P.; Lausecker, F.; Carisey, A.; Gilmore, A.; Critchley, D.; Barsukov, I.; Ballestrem, C. Relief of talin autoinhibition triggers a force-independent association with vinculinMechanisms of talin and vinculin interactions. *J. Cell Biol.* **2020**, *219* (1), e201903134.
(28) Kelley, C. F.; Litschel, T.; Schumacher, S.; Dedden, D.; Schwille, P.; Mizuno, N. Phosphoinositides regulate force-independent interactions between talin, vinculin, and actin. *eLife* **2020**, *9*, e56110.
(29) Boujemaa-Paterski, R.; Martins, B.; Eibauer, M.; Beales, C. T.; Geiger, B.; Medalia, O. Talin-activated vinculin interacts with branched actin networks to initiate bundles. *eLife* **2020**, *9*, e53990.
(30) Han, S. J.; Azarova, E. V.; Whitewood, A. J.; Bachir, A.; Guttierrez, E.; Groisman, A.; Horwitz, A. R.; Goult, B. T.; Dean, K. M.; Danuser, G. Pre-complexation of talin and vinculin without tension is required for efficient nascent adhesion maturation. *eLife* **2021**, *10*, e66151.
(31) Goult, B. T.; Zacharchenko, T.; Bate, N.; Tsang, R.; Hey, F.; Gingras, A. R.; Elliott, P. R.; Roberts, G. C.; Ballestrem, C.; Critchley, D. R. RIAM and vinculin binding to talin are mutually exclusive and regulate adhesion assembly and turnover. *J. Biol. Chem.* **2013**, *288* (12), 8238−8249.
(32) Bois, P. R.; O'Hara, B. P.; Nietlispach, D.; Kirkpatrick, J.; Izard, T. The vinculin binding sites of talin and α-actinin are sufficient to activate vinculin. *J. Biol. Chem.* **2006**, *281* (11), 7228−7236.
(33) Wang, Y.; Yan, J.; Goult, B. T. Force-dependent binding constants. *Biochemistry* **2019**, *58* (47), 4696−4709.
(34) Dahlke, K.; Zhao, J.; Sing, C. E.; Banigan, E. J. Force-dependent facilitated dissociation can generate protein-DNA catch bonds. *Biophys. J.* **2019**, *117* (6), 1085−1100.
(35) Cohen, D. M.; Chen, H.; Johnson, R. P.; Choudhury, B.; Craig, S. W. Two distinct head-tail interfaces cooperate to suppress activation of vinculin by talin. *J. Biol. Chem.* **2005**, *280* (17), 17109−17117.
(36) Johnson, R. P.; Craig, S. W. An intramolecular association between the head and tail domains of vinculin modulates talin binding. *J. Biol. Chem.* **1994**, *269* (17), 12611−12619.
(37) Chen, H.; Choudhury, D. M.; Craig, S. W. Coincidence of actin filaments and talin is required to activate vinculin. *J. Biol. Chem.* **2006**, *281* (52), 40389−40398.
(38) Izard, T.; Evans, G.; Borgon, R. A.; Rush, C. L.; Bricogne, G.; Bois, P. R. Vinculin activation by talin through helical bundle conversion. *Nature* **2004**, *427* (6970), 171−175.
(39) Izard, T.; Vonrhein, C. Structural basis for amplifying vinculin activation by talin. *J. Biol. Chem.* **2004**, *279* (26), 27667−27678.
(40) Pasapera, A. M.; Schneider, I. C.; Rericha, E.; Schlaepfer, D. D.; Waterman, C. M. Myosin II activity regulates vinculin recruitment to focal adhesions through FAK-mediated paxillin phosphorylation. *J. Cell Biol.* **2010**, *188* (6), 877−890.
(41) Stutchbury, B.; Atherton, P.; Tsang, R.; Wang, D.-Y.; Ballestrem, C. Distinct focal adhesion protein modules control different aspects of mechanotransduction. *J. Cell Sci.* **2017**, *130* (9), 1612−1624.

https://doi.org/10.1021/jacs.1c06223
J. Am. Chem. Soc. 2021, 143, 14726−14737

(42) Lemke, S. B.; Weidemann, T.; Cost, A.-L.; Grashoff, C.; Schnorrer, F. A small proportion of Talin molecules transmit forces at developing muscle attachments in vivo. *PLoS Biol.* **2019**, *17* (3), e3000057.
(43) Yao, M.; Qiu, W.; Liu, R.; Efremov, A. K.; Cong, P.; Seddiki, R.; Payre, M.; Lim, C. T.; Ladoux, B.; Mege, R.-M. Force-dependent conformational switch of α-catenin controls vinculin binding. *Nat. Commun.* **2014**, *5* (1), 1−12.
(44) Pang, S. M.; Le, S.; Kwiatkowski, A. V.; Yan, J. Mechanical stability of αT-catenin and its activation by force for vinculin binding. *Mol. Biol. Cell* **2019**, *30* (16), 1930−1937.
(45) Zhao, X.; Zeng, X.; Lu, C.; Yan, J. Studying the mechanical responses of proteins using magnetic tweezers. *Nanotechnology* **2017**, *28* (41), 414002.
(46) Berg, O. G.; von Hippel, P. H. Diffusion-controlled macromolecular interactions. *Annu. Rev. Biophys. Biophys. Chem.* **1985**, *14* (1), 131−158.
(47) Chorev, D. S.; Volberg, T.; Livne, A.; Eisenstein, M.; Martins, B.; Kam, Z.; Jockusch, B. M.; Medalia, O.; Sharon, M.; Geiger, B. Conformational states during vinculin unlocking differentially regulate focal adhesion properties. *Sci. Rep.* **2018**, *8* (1), 1−14.
(48) Lindorff-Larsen, K.; Piana, S.; Palmo, K.; Maragakis, P.; Klepeis, J. L.; Dror, R. O.; Shaw, D. E. Improved side-chain torsion potentials for the Amber ff99SB protein force field. *Proteins: Struct., Funct., Genet.* **2010**, *78* (8), 1950−1958.
(49) Mu, Y.; Nguyen, P. H.; Stock, G. Energy landscape of a small peptide revealed by dihedral angle principal component analysis. *Proteins: Struct., Funct., Genet.* **2005**, *58* (1), 45−52.
(50) Kabsch, W.; Sander, C. Dictionary of protein secondary structure: pattern recognition of hydrogen-bonded and geometrical features. *Biopolymers* **1983**, *22* (12), 2577−2637.
(51) Khan, R. B.; Goult, B. T. Adhesions Assemble!—Autoinhibition as a Major Regulatory Mechanism of Integrin-Mediated Adhesion. *Frontiers in molecular biosciences* **2019**, *6*, 144.
(52) Goult, B. T.; Xu, X.-P.; Gingras, A. R.; Swift, M.; Patel, B.; Bate, N.; Kopp, P. M.; Barsukov, I. L.; Critchley, D. R.; Volkmann, N. Structural studies on full-length talin1 reveal a compact auto-inhibited dimer: implications for talin activation. *J. Struct. Biol.* **2013**, *184* (1), 21−32.
(53) Dedden, D.; Schumacher, S.; Kelley, C. F.; Zacharias, M.; Biertümpfel, C.; Fässler, R.; Mizuno, N. The architecture of Talin1 reveals an autoinhibition mechanism. *Cell* **2019**, *179* (1), 120−131.
(54) Han, S.; Dean, K.; Whitewood, J.; Bachir, A.; Guttierrez, E.; Groisman, A.; Horwitz, A.; Goult, B.; Danuser, G. Formation of talin-vinculin pre-complexes dictates maturation of nascent adhesions by accelerated force transmission and vinculin recruitment. *bioRxiv*: 735183, **2019**.
(55) Carisey, A.; Tsang, R.; Greiner, A. M.; Nijenhuis, N.; Heath, N.; Nazgiewicz, A.; Kemkemer, R.; Derby, B.; Spatz, J.; Ballestrem, C. Vinculin regulates the recruitment and release of core focal adhesion proteins in a force-dependent manner. *Curr. Biol.* **2013**, *23* (4), 271−281.
(56) Maartens, A. P.; Wellmann, J.; Wictome, E.; Klapholz, B.; Green, H.; Brown, N. H. Drosophila vinculin is more harmful when hyperactive than absent, and can circumvent integrin to form adhesion complexes. *J. Cell Sci.* **2016**, *129* (23), 4354−4365.
(57) Auernheimer, V.; Lautscham, L. A.; Leidenberger, M.; Friedrich, O.; Kappes, B.; Fabry, B.; Goldmann, W. H. Vinculin phosphorylation at residues Y100 and Y1065 is required for cellular force transmission. *J. Cell Sci.* **2015**, *128* (18), 3435−3443.
(58) Zhang, Z.; Izaguirre, G.; Lin, S.-Y.; Lee, H. Y.; Schaefer, E.; Haimovich, B. The phosphorylation of vinculin on tyrosine residues 100 and 1065, mediated by SRC kinases, affects cell spreading. *Mol. Biol. Cell* **2004**, *15* (9), 4234−4247.
(59) Pelham, R. J.; Wang, Y.-l. Cell locomotion and focal adhesions are regulated by substrate flexibility. *Proc. Natl. Acad. Sci. U. S. A.* **1997**, *94* (25), 13661−13665.
(60) Riveline, D.; Zamir, E.; Balaban, N. Q.; Schwarz, U. S.; Ishizaki, T.; Narumiya, S.; Kam, Z.; Geiger, B.; Bershadsky, A. D. Focal contacts as mechanosensors: externally applied local mechanical force induces growth of focal contacts by an mDia1-dependent and ROCK-independent mechanism. *J. Cell Biol.* **2001**, *153* (6), 1175−1186.
(61) Gough, R. E.; Goult, B. T. The tale of two talins−two isoforms to fine-tune integrin signalling. *FEBS Lett.* **2018**, *592* (12), 2108−2125.
(62) Changede, R.; Xu, X.; Margadant, F.; Sheetz, M. P. Nascent integrin adhesions form on all matrix rigidities after integrin activation. *Dev. Cell* **2015**, *35* (5), 614−621.
(63) Gough, R. E.; Jones, M. C.; Zacharchenko, T.; Le, S.; Yu, M.; Jacquemet, G.; Muench, S. P.; Yan, J.; Humphries, J. D.; Jørgensen, C.; Humphries, M. J.; Goult, B. T., Talin mechanosensitivity is modulated by a direct interaction with cyclin-dependent kinase-1. *J. Biol. Chem.* **2021**, *297*, 100837.
(64) Goult, B. T. The Mechanical Basis of Memory−the MeshCODE Theory. *Front. Mol. Neurosci.* **2021**, *14*, 21.
(65) Khan, R. B.; Varela, L.; Cowell, A. R.; Goult, B. T. Biochemical Characterization of the Integrin Interactome. In *The Integrin Interactome*; Springer, 2020; pp 115−147.
(66) Chen, H.; Fu, H.; Zhu, X.; Cong, P.; Nakamura, F.; Yan, J. Improved high-force magnetic tweezers for stretching and refolding of proteins and short DNA. *Biophys. J.* **2011**, *100* (2), 517−523.
(67) Efron, B.; Tibshirani, R. J. *An Introduction to the Bootstrap*; CRC Press, 1994; pp 45−57.
(68) Berendsen, H. J.; van der Spoel, D.; van Drunen, R. GROMACS: a message-passing parallel molecular dynamics implementation. *Comput. Phys. Commun.* **1995**, *91* (1−3), 43−56.
(69) Abraham, M. J.; Murtola, T.; Schulz, R.; Páll, S.; Smith, J. C.; Hess, B.; Lindahl, E. GROMACS: High performance molecular simulations through multi-level parallelism from laptops to supercomputers. *SoftwareX* **2015**, *1*, 19−25.
(70) Jorgensen, W. L.; Chandrasekhar, J.; Madura, J. D.; Impey, R. W.; Klein, M. L. Comparison of simple potential functions for simulating liquid water. *J. Chem. Phys.* **1983**, *79* (2), 926−935.
(71) Ichiye, T.; Karplus, M. Collective motions in proteins: a covariance analysis of atomic fluctuations in molecular dynamics and normal mode simulations. *Proteins: Struct., Funct., Genet.* **1991**, *11* (3), 205−217.
(72) García, A. E. Large-amplitude nonlinear motions in proteins. *Phys. Rev. Lett.* **1992**, *68* (17), 2696.

https://doi.org/10.1021/jacs.1c06223
J. Am. Chem. Soc. 2021, 143, 14726−14737